Kinetic Modeling of a Comonomer Photopolymerization System Using High-Throughput Conversion Data

Peter M. Johnson,[†] Jeffrey W. Stansbury,[†,‡] and Christopher N. Bowman*[,†]

Department of Chemical and Biological Engineering, University of Colorado at Boulder, Boulder, Colorado 80309-0424, and School of Dentistry, Biomaterial Research Center, University of Colorado Health Sciences Center, Aurora, Colorado 80045-0508

Received June 21, 2007; Revised Manuscript Received October 23, 2007

ABSTRACT: A kinetic model was developed for copolymerization of (meth)acrylate formulations to optimize both kinetic parameters and predict the kinetics of unknown formulations. This model incorporates free volume theory and reaction diffusion changes in the kinetic constants as a function of conversion and reactivity ratios for the copolymerization events. High-throughput analysis data were collected for two systems as a function of composition and exposure time. Hexyl acrylate (HA) and hexanediol diacrylate (HDDA) show a nonlinear dependence on composition, with the maximum overall conversion occurring at 60 wt % HDDA. In addition, faster photopolymerization is observed as HDDA is added to a pure monoacrylate system but eventually limits the overall conversion in the system. Similar results were found with HDDA and tetrahydrofurfuryl acrylate (THFFA) with the highest conversion observed at 20 wt % HDDA. A model optimization was performed on both systems using a particle swarm optimization protocol to find the kinetic parameters which best fit the analyzed data. These optimizations show similar conversion profiles, and the optimized kinetic parameters were then used to predict conversion for a copolymerization of HA and THFFA. The monotonic increase in conversion as a function of composition is confirmed from the high-throughput data, with an average absolute error of 4.0%. A prediction of a formulation with all three monomers using the original optimized parameters and no further adjustable parameters produces a conversion profile similar to the observed profile with an average error of 5.0%.

Introduction

Photopolymerization has been a difficult polymerization pathway to characterize and model due to the kinetic complexities involved as reaction proceeds, particularly in formulations containing multiple monomers, oligomers, and additives. In the case of radical photopolymerization, generation of the radical species occurs when the initiator cleaves into a radical following absorption of ultraviolet or visible light, which initiates the polymerization. As high molecular weight polymer chains are formed along with potential cross-linking, radical termination is selectively impeded while monomer diffusion rates remain relatively high, which leads to an increase in the polymerization rate, or autoacceleration. At higher double-bond conversion, monomer mobility is also restricted, leading to a rapid decrease in polymerization as a function of conversion, or autodeceleration. This kinetic behavior makes photopolymerizations difficult to model accurately in complex, multicomponent systems. However, the advantages of photopolymerization include solvent-free systems, low power requirements, spatial control, and a wide variety of polymer chemistries, making photopolymerization useful in a large number of different fields such as dental restoratives, coatings, and photoresists.[1,2]

This wide range of applications has produced efforts into the development of photopolymerization models to predict polymerization kinetics and molecular weight distributions. Multiple groups have modeled photopolymerization kinetics in the recent past, including various factors associated with predictive shortcomings in previous models associated with photopolymerization kinetics. Research performed by Marten and Hamielec tried to predict free radical polymerization using diffusion-limited propagation and termination rate constants using the diffusivity of a small molecule through a polymer network.[3] This model employed a diffusion coefficient which was predicted to calculate styrene polymerization with thermal initiators. This model worked well in systems with little to no cross-linking or strong hydrogen bonding, limiting the variety of applicable monomer chemistries. In addition, maximum conversion was independent of cure conditions, a behavior which is significantly different from observed polymerization kinetics. A kinetic model proposed by Bowman and Peppas used critical fractional free volumes to determine the diffusion-controlled polymerization regimes.[4] This model predicted the incomplete conversion of a cross-linked system and the light intensity dependence of the maximum achievable conversion. Continuing research expanded on and refined the free volume theory, including adding reaction diffusion termination using summed reaction resistances, mass and heat transfer effects, chain length dependent termination, and oxygen inhibition.[5−12]

Here, this proposed model employs free volume dependent kinetics and incorporates the ability to copolymerize any number of monomers while simultaneously restricting the number of parameters to allow for kinetic parameter optimization using data collected from high-throughput conversion analysis. Previous work expanded the analytical model to include a variety of photopolymerization conditions and kinetic behavior but necessitated extensive experimentation to approximate the kinetic constants. Here, this work is limited to the inclusion of free volume dependent kinetics and reaction diffusion-controlled termination to limit the number of parameters per monomer. Modeling of a two-component system and the subsequent optimization of kinetic parameters requires data sets covering

* To whom correspondence should be addressed. E-mail: Christopher.bowman@colorado.edu.
[†] University of Colorado at Boulder.
[‡] University of Colorado Health Sciences Center.

10.1021/ma071383p CCC: $40.75
Published on Web 12/06/2007

large areas of the parameter space, instead of being found through experiments such as pulsed laser polymerization. These large data sets are collected rapidly through the use of high-throughput analysis techniques to analyze conversion over a broad range of compositions and exposure times. These high-throughput samples provide data points over the range of two variables, varying independent factors in an orthogonal pattern on a single substrate to determine interaction effects and for rapid property analysis. The data collection technique is automated and generates conversion for the entire range of compositions for varying exposure times in a much more rapid manner than individual testing of monomer compositions.

The development of high-throughput analysis techniques was first applied in the material science field for unique metallic semiconductors, testing a wide range of compositions within a short time frame. This approach spread to other fields, including chemistry, biology, and material science.[13,14] In the field of polymer science, techniques were first used on polymer−polymer blends annealed to a surface, producing phase behavior as a function of temperature and polymer composition.[15] Other techniques and analysis methods have been produced for surface energy measurements, adhesion, and biocompatibility.[16−21] However, most of these analyses still use copolymer blends produced from solvated polymers, not bulk monomer composition gradients.[22−24] Previous work details the development of an analysis technique to measure conversion using exposure time and monomer composition gradients using Fourier transform infrared (FTIR) spectroscopy.[25] In this paper, this high-throughput technique for analyzing composition and exposure time for photopolymers is applied to collect data to first predict kinetic constants for the copolymerization model and confirm the validity of the model and subsequently predict the conversion in two- and three-monomer copolymerizations.

Experimental Section

Materials. Hexyl acrylate (HA), hexanediol diacrylate (HDDA), and tetrahydrofurfuryl acrylate (THFFA) were obtained from Aldrich (Milwaukee, WI). The photoinitiator dimethoxyphenylacetophenone (DMPA) was obtained from Ciba-Geigy (Hawthorn, NY). All purchased reagents were used without further purification.

Exposure Time and Composition Gradients. The methodology for exposure time and composition gradients was explained in detail elsewhere, but a brief overview of each gradient is described here. Composition gradients are produced using a microfluidic mixer with control of the composition dependent on the monomer flow rates. This composition gradient is deposited onto a NaCl salt crystal substrate which is then spread orthogonally across the substrate. A second salt crystal laminates the sample, limiting the oxygen to the amount dissolved into the monomer solution and also produces a constant laminate thickness across the surface for more consistent FTIR analysis. Analyzed samples confirm no statistical difference in composition orthogonal to the composition gradient.

The exposure time gradient is produced using a cover plate attached to a linear motion stage that moves over the sample, sequentially blocking regions of the monomer from the light. The ultraviolet light source (Novacure, 100 W Hg short-arc lamp, EXFO, Mississaugua, Ontario, Canada) is placed above the sample, using a light guide with a single lens collimator. The exposure time gradient is then generated orthogonal to the composition gradient, producing a sample with varied compositions and exposure times. The exposure time plate is positioned to retain a region of no exposure to ultraviolet light. During exposure, the plate moves at a fixed rate across the sample. The exposure time for each position is determined from the speed of the plate and the region of unexposed distance on the sample. A typical prepared sample for this analysis had an exposure time gradient from 0 to 24 s, with a composition gradient from 0/100 to 75/25 wt % of a two-monomer mixture. Multiple composition gradients were produced and analyzed to ensure the entire range of comonomer formulations was represented adequately and with overlap prior to optimization of the kinetic parameters.

High-Throughput Conversion Analysis. The methodology to analyze the gradient sample has been explained previously, but briefly, the sample is placed in a Fourier transform infrared (FTIR) microscope (Nicolet Continuum) after both gradients have been generated on the sample.[25] FTIR spectra were measured at 4 cm^{-1} resolution at 4 scans per point using the IR microscope. A rectangular grid of points is placed on the sample; the microscope samples each of these points sequentially. A grid of 234 points takes 45 min to complete. This analysis corresponds to 9 composition rows with 26 exposure time columns per sample substrate. The microscope aperture is 100 μm square, with an aperture variation of 0.2 s in the time direction and a maximum of 0.5 wt % in the composition gradient direction.

The positions of the sample edges and each grid point are known, allowing for exposure time to be calculated for each IR spectra point taken. Conversion is determined from the carbon−carbon double-bond peak area between 1662 and 1581 cm^{-1}, with collected spectra in the unexposed region serving as a measurement of initial double-bond concentration. Compositions are also determined from IR spectra to ensure the accuracy of the predicted gradients, with a standard error of 3.5% for HA−HDDA and 3.1% for THFFA−HDDA and HA−THFFA mixtures. Once sufficient samples have been analyzed, conversion data from rows of equivalent composition are used to determine average conversion and standard error. These compositions are then used to generate a conversion color map with axes of composition and exposure time.

Model Development

A kinetic model was developed to facilitate analysis of the copolymerization systems, including the capability to optimize kinetic parameters using high-throughput conversion analysis data. The kinetic model builds upon previous work presented in detail by Goodner and Bowman, explaining free volume dependent modeling for the kinetic parameters for a mono-(meth)acrylate system.[6] Copolymerization of multiple monomers was incorporated using reactivity ratios, and postexposure polymerization, commonly called dark polymerization, was added to simulate the conditions of the high-throughput conversion analysis technique. From mode proposed by Goodner and Bowman, the mixture's free volume is calculated from the individual component free volumes, using a volume average over all significant components. The set of equations used to describe the overall free volume in terms of species concentration is then

$$c_{Pi} = c_{Mi0} - c_{Mi} \tag{1}$$

$$v_T = \sum_{i=1}^{n} \left(\frac{c_{Mi} M_{Mi}}{\rho_{Mi}} + \frac{c_{Pi} M_{Mi}}{\rho_{Pi}} \right) \tag{2}$$

$$\phi_{Mi} = \frac{c_{Mi} M_{Mi}}{\rho_{Mi} v_T} \tag{3}$$

$$\phi_{Pi} = \frac{c_{Pi} M_{Mi}}{\rho_{Pi} v_T} \tag{4}$$

$$f = 0.025 + \sum_{i=1}^{n} \phi_{Mi}\alpha_{Mi}(T - T_{GMi}) + \phi_P\alpha_P(T - T_{GP}) \quad (5)$$

In these equations, the concentration of monomer, c_{Mi}, volume fraction of each monomer, ϕ_{Mi}, the molecular weight, M_{Mi}, and monomer density, ρ_{Mi}, are all known or calculated parameters for monomer i. The initial concentration of monomer, c_{Mi0}, is used to determine the concentration of polymer, with the density of that polymer fraction, ρ_{Mi}. The parameter υ_T is a normalized total volume calculated to ensure volume fractions, ϕ_i, sum to unity. The polymer volume fractions are combined into a single polymer fraction, with a polymer glass transition temperature, T_{GP}, estimated using the weight fraction of monomer and individual polymer glass transition temperatures. Coefficients of thermal expansion for the monomer and polymer are α_{Mi} and α_{Pi}, respectively, and the glass transition temperature of the monomer is denoted as T_{GMi}. Free volume is calculated from a volume average of the fractional free volume of the individual monomers and the polymer.

The propagation and termination kinetic constants used in this work include Arrhenius temperature dependence, with resistances associated with both diffusion and reaction−diffusion kinetics. These kinetic parameters are given in eqs 6 and 7, respectively.[9,26]

$$k_p = k_{p0}\exp(-E_{Ap}/R_{gas}T)(1 + \exp(A_p(1/f - 1/f_{cp})))^{-1} \quad (6)$$

$$k_t = k_{t0}\exp(-E_{At}/R_{gas}T) \times \left(1 + \frac{1}{R_{rd}k_p[M_{tot}]/(k_{t0}\exp(-E_{At}/RT)) + \exp(A_t(1/f - 1/f_{ct}))}\right)^{-1} \quad (7)$$

k_{p0} is the pre-exponential kinetic factor, representing the kinetic parameter in the absence of any mass transfer restrictions for propagation through unreacted carbon−carbon double bonds of the same monomer type. Similarly, k_{t0} is the pre-exponential kinetic constant for the bimolecular termination reaction of two radicals. E_{Ap} and E_{At} are the Arrhenius-based activation energies for propagation and termination, respectively. f is the fractional free volume of the polymerizing solution calculated in eq 5; f_{cp} and f_{ct} are the critical fractional free volumes where propagation and termination start to become diffusion-controlled, respectively. A_p and A_t govern the rate at which propagation and termination decrease when the reaction is diffusion-controlled. Other parameters include the reaction−diffusion parameter, R_{rd}, the concentration of any unreacted double bonds, M_{tot}, and the gas constant, R_{gas}. If the polymerization occurs at a different temperature, the critical free volumes change as a function of temperature, according to eq 8:[6]

$$\frac{1}{f_c} = \frac{1}{f_c^{ref}} + \frac{E_A}{AR}\left(\frac{1}{T} - \frac{1}{T_{ref}}\right) \quad (8)$$

Equation 8 works for both diffusion-limited processes, so the subscripts for propagation or termination are dropped. If a critical free volume, f_c^{ref}, is known at one temperature, T_{ref}, a critical free volume at another temperature is readily estimated.

With this modeling approach, the addition of copolymerization mechanisms significantly expands the number of possible events that occur. Propagation and termination events are dependent on the radical and monomer type with individual kinetic constants for each pairing. Dissolved oxygen, Z, is also included in the model, and the peroxide radicals formed are assumed to be inert over the time span of the model. Since the samples are laminated, dissolved oxygen is not replenished due to diffusion and this inhibition delays the buildup of propagating radicals in the polymerization.

$$I + h\upsilon \xrightarrow{R_i} 2R^{\bullet} \quad (9.1)$$

$$R^{\bullet} + M_i \xrightarrow{k_i} P_i^{\bullet} \quad (9.2)$$

$$P_i^{\bullet} + M_j \xrightarrow{k_{pij}} P_j^{\bullet} \quad (9.3)$$

$$P_i^{\bullet} + P_j^{\bullet} \xrightarrow{k_{tij}} P_{ij} \quad (9.4)$$

$$P_i^{\bullet} + Z \xrightarrow{k_z} P_iZ \quad (9.5)$$

In this reaction mechanism, eq 9.1 is the photolysis of the initiator and produces two primary radicals which are assumed to be of equivalent reactivity in this work. The rate of consumption of the initiator is determined by the absorption of light and is given by the following equation:

$$R_i = 2\phi\frac{-2.303\epsilon C_I I}{E'} \quad (10)$$

where ϵ is the molar absorptivity of the initiator, C_I is the photoinitiator concentration, and I is the light intensity in mW/cm^2. E' is the energy per mole of photons and is dependent on the wavelength of the illumination source. This value converts the power density given by I into a molar rate for the decomposition of initiator. In this equation, the 2 arises since in most photocleaving initiators two radicals are produced per initiator molecule, and ϕ is the product of the efficiency and quantum yield.

The second step, shown in eq 9.2, is the chain initiation process. In this reaction a primary radical reacts with a monomer of type i (M_i) to form a polymer chain ($P_i^{\bullet}$). The rate of this reaction is determined by the kinetic constant for chain initiation, k_i. In this model, k_i is equivalent to a primary radical reaction with any monomer unit. The propagation reactions are represented by eq 9.3, with the kinetic constant of propagation represented as k_{pij}. With multiple monomers, copolymerization between radicals and monomers of different and the same type will occur. The ij subscript denotes a propagation constant where the radical of type i reacts with a double bond of type j to form a new polymer radical of type j. The number of propagation reactions is the square of the number of polymerizable species in the formulation, as each radical type can polymerize with the same type or any other type of monomer in the system.

Kinetic analysis of propagation in a two-component system requires four values for all conversions, so reactivity ratios are used to simplify the optimization in all multicomponent systems.[27,28] In a two-component system, reactivity ratios, r_{12} and r_{21}, are shown in eqs 11a and 11b. When the model contains more than two monomers, additional r_{ij} values are required as needed.

$$r_{12} = k_{p11}/k_{p12} \quad (11a)$$

$$r_{21} = k_{p22}/k_{p21} \quad (11b)$$

With the monomers used in this study, since each monomer contains only acrylate functional groups, the reactivity ratios should be near unity as all three monomers lack of hydrogen bonding or any additional monomer backbone chemistry known to produce systems with high reactivity. Therefore, reactivity ratios are assumed to be constant and equal to one throughout the polymerization though it is readily possible to adjust this value.

The final step in polymerization is termination, denoted by a kinetic constant k_{tij}. Each radical terminates with any other polymer radical in the system, with subscript *ij* denoting the two contributing species types terminating. If dissimilar radicals are terminating, an average of their termination kinetic constants is used. The termination kinetic constant contains both the free volume resistance and a reaction−diffusion resistance, a mechanism which predominately occurs when the system is at a high conversion and pendant radicals have limited mobility. The trapped radical must diffuse through propagation events to reach another radical and terminate.

Each distinct composition and exposure time data point collected from the high-throughput analysis technique is initially modeled without dark polymerization. After the kinetic model is completed, these data are then used to determine postexposure polymerization, commonly called dark polymerization, at each time point. Since the high-throughput analysis is an ex-situ measurement of conversion, polymerization will continue even after the irradiation is ceased. Following irradiation, radicals still exist and until terminated have the ability to propagate through unreacted double bonds. The additional conversion associated with dark polymerization is significant in highly cross-linked systems during autoacceleration. Therefore, a calculation of this additional conversion is required to model the determined conversion from the high-throughput analysis.

Computationally, solving the differential equations associated with dark polymerization for each exposure time and composition sample point is impractical, particularly while the model is optimizing parameters. Therefore, dark polymerization is determined using a semiempirical formula based on equations for a single monomer under the same conditions. The dark polymerization of a two-monomer, two-radical system cannot be solved analytically, so the system was reduced to a lumped single-radical, single-monomer system to estimate the kinetics following the cessation of irradiation. This equation assumes constant k_p and k_t over the span of the dark polymerization, since the conversion change in most cases is not sufficient to affect the free volume and consequently the kinetic parameters. The dark polymerization equation uses lumped parameters for k_p and k_t, as shown in eq 12. For single-monomer systems, this equation will revert to the correct form for dark polymerization of a single monomer.[7,9]

$$M_{tot} - M_{tot,0} = \frac{k_{pL} M_{tot}}{2k_{tL}} \ln(2k_{tL} R_0 t + 1) \qquad (12)$$

R_0 is the sum of both radical concentrations when the light is shut off, while k_{pL} and k_{tL} are the lumped kinetic parameters. These lumped parameters are weighted using the volume fractions of the monomer concentration at that point in time. M_{tot} is the total double-bond concentration at *t*, the total time after the light has been shut off. $M_{tot,0}$ is the concentration at the point the light exposure ceases. Comparing the differential equation model of the system to the semiempirical formula, the dark polymerization results proceed differently vs time. A majority of the dark polymerization will have occurred by the time the sample is placed for analysis, which means the only relevant conversion is the conversion at long times. The difference in conversion between the differential equation model and the lumped parameter model at long times is different by at most 10% of the conversion which is associated with dark polymerization. Since dark polymerization in these systems rarely exceeds 10% of the total conversion, this error is minor in comparison to the other assumptions included in the model. In addition, only HDDA shows significant dark polymerization due to a much steeper autoacceleration and does not affect a large portion of the parameter space.

The kinetic model described above was programmed in MATLAB with a graphic interface, using an ordinary differential equation solver over the time range required. The solver uses a trapezoidal step solver, which works for stiff sets of equations. This method is required as the initial distribution of points in the parameter optimization could have parameters leading to stiff equations that will slow the differential equation solver down further. A more rigorous analysis of the solver shows less than 0.1% conversion change in conversion as a function of time for any of the differential equation solvers. A graphic interface was also designed to allow the data sets to be loaded and parameters changed before each model run.

The optimization protocol uses a particle swarm optimization procedure, used in a variety of continuous functions.[29,30] The algorithm is based off a search of randomly dispersed points within a parameter space, which moves in the search space with a velocity dynamically adjusted dependent on the current optimal position and its own previous positions. The points, or particles, all tend toward the optimal global point but travel through the rest of the parameter space. The calculation is optimized using a sum-squared error of the entire parameter space for all 12 kinetic parameters simultaneously. Since this optimization system has several interdependent parameters, this optimization technique allows for a random search throughout a large portion of the parameter space. Each individual particle is represented as three arrays where *j* corresponds to the number of dimensions in the optimization. $X_i = (x_{i1}, x_{i2}, ..., x_{ij})$ is the current position of the particle, and $V_i = (v_{i1}, v_{i2}, ..., v_{ij})$ is the velocity of the particle. Both of these arrays are randomly seeded for every particle. The best global position with the lowest optimization value is $P_g = (p_{g1}, p_{g2}, ..., p_{gj})$, with $P_i = (p_{i1}, p_{i2}, ..., p_{ij})$ as the best previous position for every particle in the system. The parameters of each particle are used, and the conversion results from the model are compared to the data. The error between the data and model is calculated and compared to the previous best optimization point for that particle and the global particle. P_g and P_i are updated if necessary, and new velocities and positions are generated from the following equations:

$$v_{id} = wv_{id} + c_1 \text{rand}(\,)(p_{id} - x_{id}) + c_2 \text{rand}(\,)(p_{gd} - x_{id}) \qquad (13)$$

$$x_{id} = x_{id} + v_{id} \qquad (14)$$

where *w* is an inertial weighting factor that decreases with number of flights taken, and c_1 and c_2 are two positive constants. The rand( ) function is two separate random number generators with a range of [0,1].

After each particle has moved, the parameters at each particle point are used to analyze the kinetic model at all compositions and compared to the collected high-throughput data. The error is calculated, and P_i and P_g are updated if the error at these points is less than the current values. These steps repeat until a minimum has been found. This model uses 196 particles, with

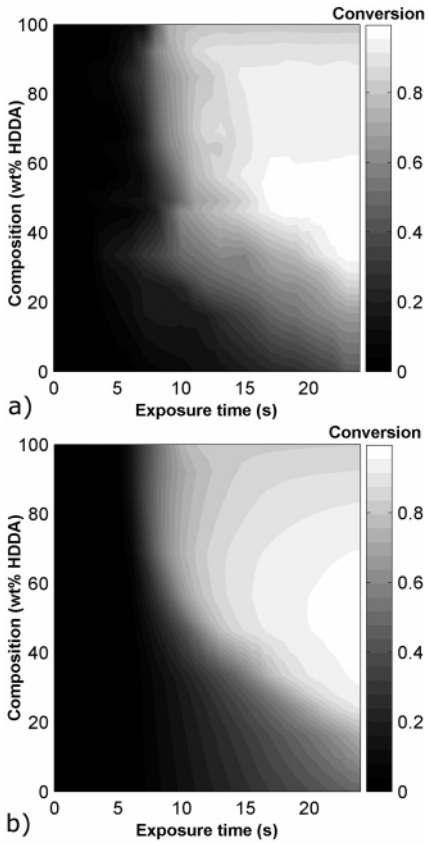

Figure 1. HA−HDDA conversion color map for the high-throughput analysis **(**a**)** and the optimized model **(**b**)**. Samples were polymerized at a light intensity of 5.0 mW/cm^2 with 0.5 wt % DMPA at 23 °C using an exposure time gradient from 0 to 24 s. Modeling was performed at the same conditions, with time and composition points matching all points of the high-throughput data plot.

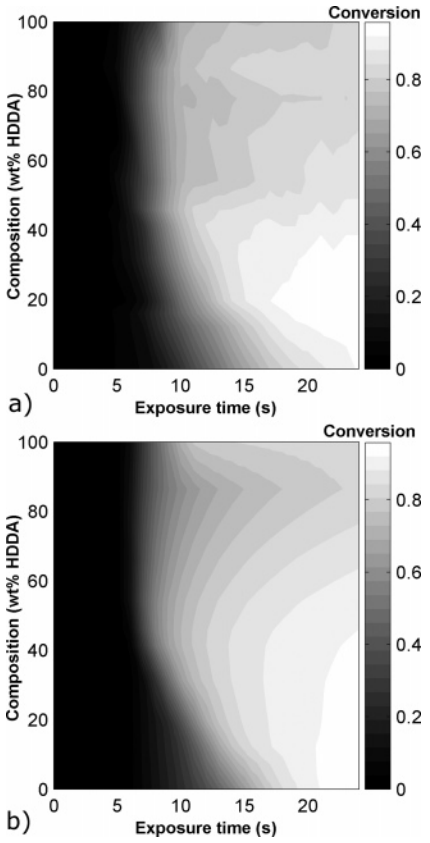

Figure 2. THFFA−HDDA conversion color map for the high-throughput analysis **(**a**)** and the optimized model **(**b**)**. Samples were polymerized at a light intensity of 5.0 mW/cm^2 with 0.5 wt % DMPA at 23 °C using an exposure time gradient from 0 to 24 s. Modeling was performed at the same conditions, with time and composition points matching all points of the high-throughput data plot.

$c_1 = 0.5$ and $c_2 = 0.5$. The inertial weighting factor was varied from 0.5 to 0.8 dependent on the size of the parameter space. Results found in this paper used a parameter space limited to a range of ±20% of the initial values with a weighting factor of 0.6, since expansion of the searchable space to larger values led to particles located at systems with computationally stiff equations. The kinetic parameters for the initial values were determined from previous monomer analysis from the literature and subsequent manual optimization to ensure the initial estimate was similar to the conversion found in the data.

Once the optimization ends, the final results are tested, and an error plot is produced to ensure that the error is distributed randomly. If the error is not distributed randomly, the optimization is run again. In the case of HDDA, the parameters were determined independently from the copolymerizations with each of the different monoacrylates, and the parameters were found to be similar for HDDA from either of these two independent data sets. THFFA and HA kinetic parameters were found using the copolymerization data with HDDA, using their respective data sets.

Results

HA/HDDA and THFFA/HDDA Optimization. High-throughput analysis of composition gradients containing HDDA with a single monoacrylate was performed to produce the results required for the kinetic parameter search. The data set containing a HA/HDDA composition gradient was analyzed first, with the high-throughput data color map in Figure 1a and the model result in Figure 1b. The color map uses the pcolor function in MATLAB to produce a color contour map of the conversion data points, with the color bar on the left as a legend to determine individual color contours. The second composition gradient of HDDA and THFFA was analyzed at the same conditions and is shown in Figure 2a with the corresponding model prediction in Figure 2b. The kinetic constants for HDDA are the same parameters in both cases, as the individual modeling of both systems produces conversion profiles with changes of at most 1% throughout the polymerization. The kinetic parameters themselves were within 5%, and an average of these parameters was used in the model of both systems. The averaging of these kinetic parameters did not significantly affect the conversion kinetics of either color map.

In both cases, the high-throughput analysis exhibits a nonlinear change in kinetics, with the highest ultimate conversion observed at an intermediate comonomer mixture. The model is successfully able to predict the nonlinearity for both systems and also to determine the point at which slower kinetics begin to appear due to the addition of the monoacrylate. Table 1 shows the property parameters for each monomer and their optimized kinetic constants used in the copolymerization kinetic model, with the values labeled in bold.

The parameters derived for this model compare well with data collected from laser pulse experiments to determine values for k_p for monoacrylates. For other alkyl acrylates, k_p at low conversion has been calculated to lie within a range of 16 000−18 500 L mol^{-1} s^{-1} dependent on the acrylate and experimental setup.[31,32] No specific data could be found for hexyl acrylate, but the predicted k_p at low conversion using the model is 17 500 L mol^{-1} s^{-1}, well within the range of independently determined

Table 1. Parameters Used for Modeling HDDA, HA and THFFA, Including Optimized Parameters. References Denote the Source of Additional Parameters

parameter	units	HDDA	HA	THFFA	ref
MW	g/mol	228	156.1	156.1	
ρ_m	g/mL	1.010	0.888	1.063	
ρ_p	g/mL	1.29	1.03	1.29	Painter and Coleman[33]
T_{gm}	K	278	228	213	from T_m
T_{gp}	K	450	245	261	experimentally determined
E_{Ap}	J/mol	18230	18230	18230	Goodner et al.[6]
E_{At}	J/mol	2970	2970	2970	Goodner et al.[5]
			From Model Optimization		
k_{p0}	L/mol s	3.15×10^7	3.04×10^7	3.11×10^7	
k_{t0}	L/mol s	6.35×10^7	6.46×10^7	6.22×10^7	
f_{cp}		0.0212	0.034	0.0391	
f_{ct}		0.049	0.048	0.059	
A_p		1.2	0.37	0.41	
A_t		3.1	0.56	0.72	
			Additional Constants		
α_m	1/°C	0.0005			Goodner et al.[5]
α_p	1/°C	0.00075			Goodner et al.[5]
ϕ		0.6			Goodner et al.[5]
ϵ	L/mol s	150			Goodner et al.[5]
R	L/mol	4			Anseth et al.[7]
r_{ij}		1			
R_{gas}	J/mol K	8.314			
k_z	L/mol s	3.2×10^8			Goodner et al.[5]

Table 2. Error Analysis of Model Parameters

parameter	HDDA (HA)	HDDA (THFFA)	HA	THFFA
k_{p0}	3.3×10^7, 3.5×10^7	3.3×10^7, 3.6×10^7	3.0×10^7, 3.2×10^7	3.0×10^7, 3.2×10^7
k_{t0}	6.0×10^7, 6.5×10^7	6.1×10^7, 6.4×10^7	6.10×10^7, 6.3×10^7	6.10×10^7, 6.3×10^7
f_{cp}	0.0205, 0.0213	0.0204, 0.0215	0.034, 0.035	0.0390, 0.0395
f_{ct}	0.0486, 0.0504	0.0486, 0.0499	0.048, 0.049	0.059, 0.061
A_p	1.13, 1.23	1.17, 1.25	0.35, 0.37	0.42, 0.45
A_t	3.1, 3.2	3.0, 3.2	0.55, 0.57	0.71, 0.73

propagation constants. In addition, the dark polymerization is a significant factor in the model, showing a 10% increase in conversion for pure HDDA samples. The monoacrylates show less than 1% conversion in the dark due to more facile termination in the absence of cross-linking and are within the range of expected dark polymerization for a monoacrylate.

Error analysis of the optimized kinetic parameters was performed using the particle swarm optimization. The optimized sum squared error of the model is used as the lower limit, and an increase of 4% of the sum squared error was used to calculate the upper limit. The kinetic parameters for each monomer were analyzed separately, and the particles were tracked throughout the optimization. In the case of THFFA−HDDA, kinetic parameters were stored when the sum-squared error was calculated between 0.536 and 0.553. The kinetic parameters from this analysis were used to determine the error intervals for the six optimized parameters. This method produces an upper and lower limit to each kinetic parameter at which the sum-squared error will be within 4% of the minimum error. The HDDA kinetic parameter error interval using both conversion data sets is shown in Table 2, along with the error interval for both monoacrylates.

The HDDA predictions in both systems are within the same error ranges, and parameters from the HDDA−HA system were used in both cases. The error between the model and the analyzed data shows a maximum error of 31% for the HA/HDDA data set, with an average absolute error of 5.5%. A majority of the error in this system comes from a few compositions, all located between 20 and 50 wt % HDDA. This region shows a much larger autoacceleration regime in the modeled results which is not evident in the high-throughput data. Compositions outside of that range are predicted more accurately, except for pure HDDA at the points where autoacceleration occurs. In the case of THFFA/HDDA, the maximum error is 14.4%, with an average absolute error of 3.3%. If the optimized parameters for THFFA/HDDA are used, the average absolute error is 3.2%, with a maximum error of 13.2%, an insignificant change. Error in this system is caused in the same region as above, but showing a better prediction overall. In both cases, however, the predicted results show the same trends in polymerization conversion as a function of both composition and exposure time. The maximum observed conversion occurs in the same regions in both the model and the analyzed data, and the onset of significant conversion as a function of composition is similar.

HA−THFFA Predicted Conversion and Comparison to High-Throughput Data. From the results described above, kinetic parameters from HA and THFFA were found. Using these parameters, copolymerization of HA and THFFA was modeled before a high-throughput analysis of the comonomer mixture was performed. The monoacrylate kinetic parameters used in this conversion prediction were from the copolymerization data for HDDA. Optimization of all kinetic parameters was done with only the HA/HDDA and THFFA/HDDA data sets. The model result shows a monotonic increase in photopolymerization kinetics as the amount of THFFA increases within the sample. This high-throughput conversion analysis is shown in Figure 3a, with the model prediction in Figure 3b. Figure 4 presents the conversion color map obtained from the high-throughput analysis. The maximum deviation from the model is 14%, with an average absolute deviation of 4%. Most of this error is from a steeper decrease in the HA conversion kinetics, which propagates through the rest the rest of the kinetics in this system.

In both cases, a monotonic increase in the photopolymer conversion is seen with increasing THFFA. The predicted color

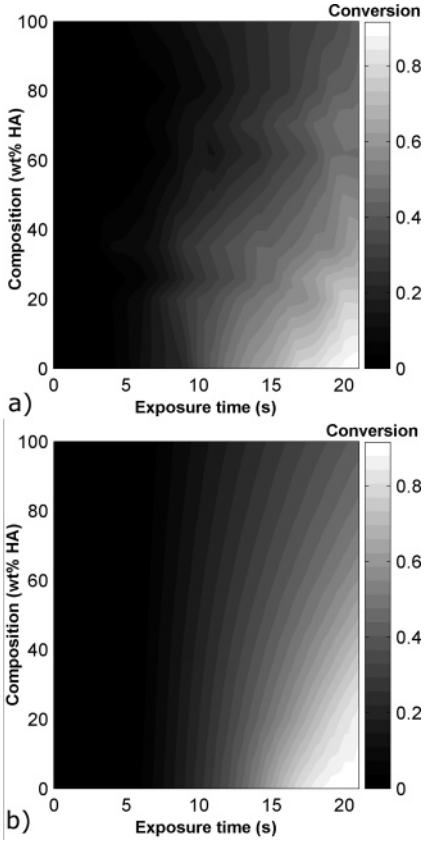

Figure 3. THFFA−HA conversion color map for the high-throughput analysis **(**a**)** and the kinetic model **(**b**)**. Samples were polymerized at a light intensity of 5.0 mW/cm^2 with 0.5 wt % DMPA at 23 °C using an exposure time gradient from 0 to 24 s. Modeling was performed at the same conditions and sample points, with kinetic parameters from the previous study with no additional optimization.

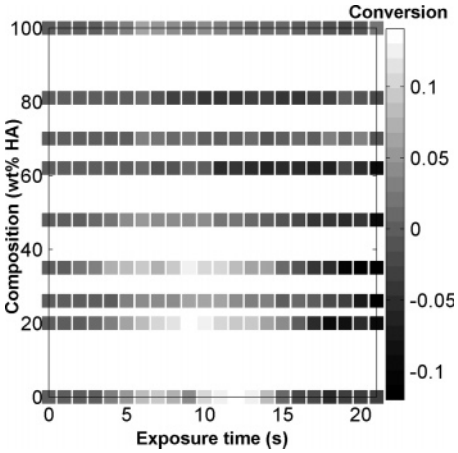

Figure 4. THFFA−HA absolute error map. Samples were polymerized at a light intensity of 5.0 mW/cm^2 with 0.5 wt % DMPA at 23 °C using an exposure time gradient from 0 to 24 s. Modeling was performed at the same conditions and sample points, with kinetic parameters from the previous study with no additional optimization.

map matches the results seen in Figure 3a, with similar conversion at the same exposure time. A plot of the conversion difference is shown in Figure 4. In Figure 4, there is no significant error over 13% conversion. The largest source of error occurs for the prediction of the HA kinetic parameters, which produces a systematic error in the predicted results. However, this model successfully predicts the copolymerization behavior while only using optimized parameters from previous analyses. The estimated parameters show significant utility in

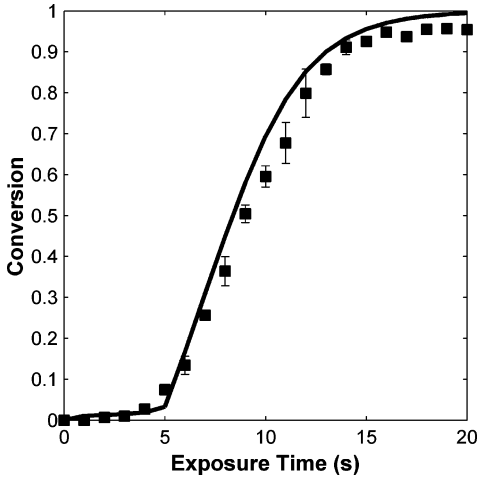

Figure 5. Conversion profiles of a three-component monomer mixture as a function of exposure time using both high-throughput analysis (squares) and the model prediction (line) at a light intensity of 5.0 mW/cm^2 with 0.5 wt % DMPA at 23 °C. The conversion profile of the 53/26/21 wt % HDDA/HA/THFFA mixture is predicted well in both the autoacceleration and autodeceleration regions.

predicting the conversion over the entire range of both exposure time and composition. Further optimization is possible, but the results shown above produce an accurate model to compare results from multiple different formulations.

Ternary Photopolymerization Modeling. The model can be expanded to three-component formulations, in this case using all three monomers already determined to produce conversion as a function of exposure time for a comonomer formulation. A formulation containing 53/26/21 wt % HDDA/HA/THFFA was polymerized under the same conditions as the previous samples. The formulation was randomly selected from a range of modeled formulations that exhibit a high conversion of the carbon−carbon double bonds prior to 20 s of exposure time. This system was then modeled and compared to the results found from the high-throughput analysis. A comparison of the two conversion profiles is shown in Figure 5.

The profiles in Figure 5 are similar, with a maximum deviation of −13.2% at 11 s of exposure time. The model prediction consistently overpredicts the monomer conversion at a given exposure time, but the profiles match at the onset of photopolymerization and the autodeceleration regime. Both systems also show a rate decrease at similar exposure times and reach nearly complete conversion at later exposure times. The average conversion error is 5.0% due to the model consistently overpredicting the conversion. The prediction of a three-monomer copolymerization proves useful as it confirms the ability to add additional components without a significant increase in the error. The overall accuracy of both the composition gradient and three-component system conversion results demonstrates the efficacy of this technique in predicting different compositions using kinetic parameters found in previous studies. The kinetic parameters were found with minimal input but were applicable to estimate and predict the conversion of unknown systems before an FTIR analysis was employed.

Conclusions

A copolymerization model was produced that allows for kinetic parameters to be estimated and optimized from high-throughput FTIR analysis using gradients of exposure time and composition. Samples analyzed using gradients of exposure time and composition are a useful technique for collection of large

data sets for model optimization. This model employs a particle swarm optimization to increase the speed of optimization and maximize the possibility of finding the best parameters. Systems containing HA/HDDA and THFFA/HDDA compositional gradients were optimized using this technique, providing kinetic parameters for each model. In both systems, the results for HDDA were nearly equivalent, showing the efficacy of the optimization route and providing credence to the parameters usefulness in modeling unknown compositions.

This accuracy was confirmed by similar conversions from the model and experiments for composition gradient of HA and THFFA. Both the model and the high-throughput analysis show a monotonic increase in the conversion as THFFA increases, with the main source of error coming from an overestimation of the HA kinetic parameters. In addition to a compositional gradient test, a three-component polymerization using all three monomers was modeled and subsequently analyzed using the same technique. The model matches well, showing similar conversion profiles to the high-throughput results. The ability to fit and then predict monomer conversion provides a means to potentially screen additional combinations of monomer mixtures once the monomer is integrated into the current framework. While there is error involved in this analysis due to the assumptions required, this model provides a pathway to determine an estimate for a conversion profile as a function of exposure time. These profiles could then be used to determine the optimal portion of the parameter space to search using the high-throughput technique, reducing the amount of experimentation and optimization time required to produce better materials for future applications.

Acknowledgment. We thank the I/UCRC for Fundamentals and Applications of Photopolymerization and the NSF GAANN fellowship for funding.

References and Notes

(1) Decker, C. *Polym. Int.* **1998**, *45* (2), 133−141.
(2) Decker, C. *Macromol. Rapid Commun.* **2002**, *23* (18), 1067−1093.
(3) Marten, F. L.; Hamielec, A. E. *J. Appl. Polym. Sci.* **1982**, *27* (2), 489−505.
(4) Bowman, C. N.; Peppas, N. A. *Macromolecules* **1991**, *24* (8), 1914−1920.
(5) Habibi, A.; Vasheghani-Farahani, E. *AIChE J.* **2004**, *50 (*6), 1260−1272.
(6) Goodner, M. D.; Bowman, C. N. *Chem. Eng. Sci.* **2002**, *57* (5), 887−900.
(7) Anseth, K. S.; Decker, C.; Bowman, C. N. *Macromolecules* **1995**, *28* (11), 4040−4043.
(8) Anseth, K. S.; Kline, L. M.; Walker, T. A.; Anderson, K. J.; Bowman, C. N. *Macromolecules* **1995**, *28* (7), 2491−2499.
(9) Anseth, K. S.; Wang, C. M.; Bowman, C. N. *Polymer* **1994**, *35* (15), 3243−3250.
(10) Lovestead, T. M.; Burdick, J. A.; Ansetha, K. S.; Bowman, C. N. *Polymer* **2005**, *46* (16), 6226−6234.
(11) Berchtold, K. A.; Lovestead, T. M.; Bowman, C. N. *Macromolecules* **2002**, *35* (21), 7968−7975.
(12) Lovestead, T. M.; O'Brien, A. K.; Bowman, C. N. *J. Photochem. Photobiol. A: Chem.* **2003**, *159* (2), 135−143.
(13) Briceno, G.; Chang, H. Y.; Sun, X. D.; Schultz, P. G.; Xiang, X. D. *Science* **1995**, *270* (5234), 273−275.
(14) Xiang, X. D.; Sun, X. D.; Briceno, G.; Lou, Y. L.; Wang, K. A.; Chang, H. Y.; Wallacefreedman, W. G.; Chen, S. W.; Schultz, P. G. *Science* **1995**, *268* (5218), 1738−1740.
(15) Meredith, J. C.; Amis, E. J. *Macromol. Chem. Phys.* **2000**, *201* (6), 733−739.
(16) Smith, A. P.; Douglas, J. F.; Meredith, J. C.; Amis, E. J.; Karim, A. *Phys. Rev. Lett.* **2001**, 8701 (1).
(17) Smith, A. P.; Douglas, J. F.; Meredith, J. C.; Amis, E. J.; Karim, A. *J. Polym. Sci., Part B: Polym. Phys.* **2001**, *39* (18), 2141−2158.
(18) Mohebi, M. M.; Evans, J. R. G. *J. Am. Ceram. Soc.* **2003**, *86* (10), 1654−1661.
(19) Sormana, J. L.; Meredith, J. C. *Macromolecules* **2004**, *37* (6), 2186−2195.
(20) Sormana, J. L.; Meredith, J. C. *Mater. Res. Innovations* **2003**, *7* (5), 295−301.
(21) Crosby, A. J. *J. Mater. Sci.* **2003**, *38* (22), 4439−4449.
(22) Sormana, J. L.; Chattopadhyay, S.; Meredith, J. C. *Rev. Sci. Instrum.* **2005**, *76* (6).
(23) Chisholm, B. J.; Christianson, D. A.; Webster, D. C. *Prog. Org. Coat.* **2006**, *57* (2), 115−122.
(24) Lin-Gibson, S.; Landis, F. A.; Drzal, P. L. *Biomaterials* **2006**, *27* (9), 1711−1717.
(25) Johnson, P. M.; Reynolds, T. B.; Stansbury, J. W.; Bowman, C. N. *Polymer* **2005**, *46* (10), 3300−3306.
(26) Anseth, K. S.; Bowman, C. N.; Peppas, N. A. *J. Polym. Sci., Part A: Polym. Chem.* **1994**, *32* (1), 139−147.
(27) Abdollahi, M.; Sharifpour, M. *Polymer* **2007**, *48* (1), 25−30.
(28) Zetterlund, P. B.; Takenaka, M.; Johnson, A. F. *Macromolecules* **2005**, *38* (6), 2173−2179.
(29) Trelea, I. C. *Inf. Process. Lett.* **2003**, *85* (6), 317−325.
(30) Bo, Z. An improved particle swarm optimization algorithm for global numerical optimization. In *Comput. Sci.—ICCS 2006, Pt. 1, Proc.* **2006**, *3991*, 657−664.
(31) Beuermann, S.; Buback, M. *Prog. Polym. Sci.* **2002**, *27* (2), 191−254.
(32) Asua, J. M.; Beuermann, S.; Buback, M.; Castignolles, P.; Charleux, B.; Gilbert, R. G.; Hutchinson, R. A.; Leiza, J. R.; Nikitin, A. N.; Vairon, J. P.; van Herk, A. M. *Macromol. Chem. Phys.* **2004**, *205* (16), 2151−2160.
(33) Graf, J. F.; Coleman, M. M.; Painter, P. C. *J. Phys. Chem.* **1991**, *95* (17), 6710−6723.

MA071383P